1   Assessing PM$_{2.5}$ Exposures with High Spatio-

2   Temporal Resolution across the Continental

3   United States

4   *Qian Di [†]*, Itai Kloog [†,‡], Petros Koutrakis [†], Alexei Lyapustin [§], Yujie Wang [§], Joel*

5   *Schwartz [†]*

6   [†] Department of Environmental Health, Harvard T.H. Chan School of Public Heath,

7   Boston, MA, 02115, USA

8   [§] GEST/UMBC, NASA Goddard Space Flight Center, Baltimore, MD, USA

11

12

1

13   ABSTRACT. A number of models have been developed to estimate $PM_{2.5}$ exposure,

14   including satellite-based aerosol optical depth (AOD) models, land-use regression or

15   chemical transport model simulation, all with both strengths and weaknesses. Variables

16   like normalized difference vegetation index (NDVI), surface reflectance, absorbing

17   aerosol index and meteoroidal fields, are also informative about $PM_{2.5}$ concentrations.

18   Our objective is to establish a hybrid model which incorporates multiple approaches and

19   input variables to improve model performance. To account for complex atmospheric

20   mechanisms, we used a neural network for its capacity to model nonlinearity and

21   interactions. We used convolutional layers, which aggregate neighboring information,

22   into a neural network to account for spatial and temporal autocorrelation. We trained the

23   neural network for the continental United States from 2000 to 2012 and tested it with left

24   out monitors. Ten-fold cross-validation revealed good model performance with total R^2

25   of 0.84 on the left out monitors. Regional R^2 could be even higher for the Eastern and

26   Central United States. Model performance was still good at low $PM_{2.5}$ concentrations.

27   Then, we used the trained neural network to make daily prediction of $PM_{2.5}$ at 1 km×1

28   km grid cells. This model allows epidemiologists to access $PM_{2.5}$ exposure in both the

29   short term and the long term.

30

2

1. Introduction

31
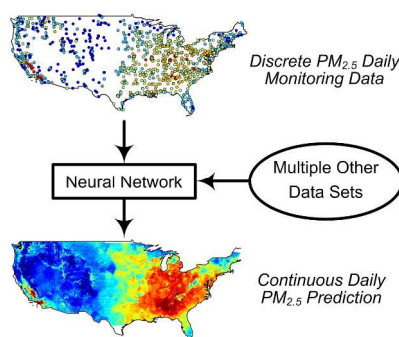
32　　Fine particulate matter ($PM_{2.5}$) is a major concern in public health.[1-6] Adverse health

33　effect is associated with $PM_{2.5}$ exposure in the short term[7,8] and the long term.[9,10] $PM_{2.5}$

34　is found to be associated with morbidity,[11,12] mortality,[6] cardiovascular disease,[4]

35　respiratory disease,[13] myocardial infarction,[14] an increase in hospital admission[11,15,16]

36　and others.[17]

37　　Accurate exposure assessment of $PM_{2.5}$ is a prerequisite of to investigate its adverse

38　health effect. Early studies estimated $PM_{2.5}$ at the nearest monitoring station.[18] However,

39　nearest monitors cannot capture all variability in $PM_{2.5}$ concentrations and non-

40　differential misclassification occurs.[19]

41　　Various approaches have been developed to achieve better exposure assessment.

42　Spatial interpolation, including nearest-neighbor interpolation and Kriging interpolation,

43　was used to smooth $PM_{2.5}$ concentration and estimate local exposure. Nonetheless,

44　interpolation adds no additional information to the model. Local emission like highways

45　between two monitor sites is not captured by simple interpolation. Land-use regression

46　(LUR) uses land-use terms, such as road density, percentage of urban and others, as

47　proxies for $PM_{2.5}$ concentration.[20,21] Although LUR could achieve a high spatial

48　resolution, it has limited temporal resolution since land-use terms are usually time-

49　invariant.[22] Recent improvements in land-use regression enable to incorporate some level

50　of time-variant factors,[23,24] but land-use terms are still inadequate in modeling short-term

51　variations and often limited by short temporal coverage.[25]

3

52   Satellite-based aerosol optical depth (AOD) measurements have been widely used to

53   estimate $PM_{2.5}$ in various models for its large spatial coverage and repeated daily

54   observations.[26] AOD measures the light extinction due to aerosol in the whole

55   atmospheric column.[27] To obtain ground-level $PM_{2.5}$ concentration, vertical distribution

56   of aerosol is needed. Recent studies proposed different calibration methods.[26, 28-32] Most

57   studies focused on quantifying relationship between AOD and $PM_{2.5}$ or predict long-term

58   average of $PM_{2.5}$, while epidemiological studies also need short-term $PM_{2.5}$ assessment.

59   Some studies combined AOD and land-use regression and used mixed effect model to

60   achieve improvements on model performance.[33-35] However, the drawback of AOD is

61   missing data, which is caused by bright surfaces or cloud contamination, especially in

62   winter.[36] Also, AOD measurements may also have abnormally large values caused by

63   forest fires.[37] For grid cells with missing or abnormal values, the AOD-$PM_{2.5}$ relationship

64   may be problematic, especially for daily $PM_{2.5}$ assessment. The relationship between

65   column aerosol concentration and ground-level concentration can be influenced by

66   multiple factors such as meteorological fields, chemical profile of aerosol and others.[38, 39]

67   Absorbing aerosol index (AAI) provides information about aerosol type and is

68   informative to $PM_{2.5}$ modeling.[40, 41]

69   Chemical transport models (CTMs), like GEOS-Chem,[42] CMAQ,[43] and CHIMERE,[44]

70   simulate the formation, dispersion and deposition of fine particles based on emission

71   inventories and known atmospheric chemical reaction. CTM is another way to assess

72    $PM_{2.5}$ concentration. Due to the complexity of reactions and atmospheric meteorological

73   processes, simulated concentration often deviates from the real world. CTM outputs are

74   often used after calibration.[45, 46] CTM provides aerosol vertical profile, which has been

4

75　used as scaling factor in AOD calibration.[29, 47] Due to the limit of computation, CTM

76　usually has coarse spatial resolution. In a previous study, we have proposed a hybrid

77　model which uses land-use regression to downscale CTM outputs. [48]

78　　　Existing approaches have both strengths and weaknesses and often they complement

79　to each other. In this paper, we incorporated multiple variables into a neural network-

80　based hybrid model, including satellite-based AOD data, AAI, CTM outputs, land-use

81　terms and meteorological variables. We validated the model with ten-fold cross-

82　validation and predicted daily $PM_{2.5}$ at 1 km×1 km resolution in the continental United

83　States for the years 2000-2012. Prediction with such a high temporal and spatial

84　resolution allows epidemiological studies to estimate health effect of $PM_{2.5}$ with greater

85　reliability.

86　**2.　Materials**

87　　**2.1. Study Domain**

88　　　The study domain is the continental United States, including 48 contiguous states and

89　Washington D.C (Figure S1). The study period is from January 1st, 2000 to December

90　31st, 2012, in total of 4,749 days.

91　　**2.2. Monitoring Data**

92　　　Monitoring data for $PM_{2.5}$ were collected by EPA Air Quality System (AQS). In total,

93　there were 1,986 monitor stations available in this period and 1,928 of them were located

94　in the study area. Not every monitoring site has data available throughout the study

95　period. Monitoring sites were densely distributed along coastal areas and the Eastern part,

5

96   while there were few monitors in the Mountain Region (Figure S1). We calibrated our

97   hybrid model to the daily average of monitored $PM_{2.5}$.

98   **2.3. AOD Data**

99   The Moderate Resolution Imaging Spectroradiometer (MODIS) is an instrument

100   aboard the Earth Observing System (EOS) satellite.[49, 50] Several algorithms have been

101   developed to retrieve AOD data from MODIS measurement,[51] including a recent

102   algorithm called MAIAC, which retrieves AOD with a spatial resolution of 1 km×1 km.

103   [52-54] We used MAIAC AOD data from Aqua satellite from 2003 to 2012 and Terra

104   satellite from 2001 to 2012. MAIAC algorithm arranges data at 600 km×600 km tile,

105   which includes 360,000 1 km×1 km grid cells. In total 33 tiles and 11,880,000 grid cells

106   were used in this study, which is also the grid cell we made predictions at. Grid cells over

107   water bodies were excluded from the study.

108   AOD data has some portion of missing values, especially in the winter. Missing

109   values are caused by bright surfaces (e.g. snow coverage) and cloud contamination.[36] In

110   addition, AOD data may have abnormally large values due to extreme events like forest

111   fires.[37] Usually AOD data with values above 1.5 are excluded from modeling, which also

112   creates missing values.[55] Our previous study calibrated column aerosol mass from CTM

113   outputs to satellite-based AOD and predicted AOD values when satellite-based AOD are

114   missing.[56] For AOD data used in this study, we filled in the missing values using this

115   method as pre-processing (Section 3, Supplementary Material).

116   **2.4. Surface Reflectance**

6

117   Surface characteristics and errors in AOD data products have been well documented

118   by previous studies.[57] MAIAC algorithm was designed to retrieve AOD over various

119   surfaces, but surface brightness can still affect data quality.[54] We used MODIS surface

120   reflectance data (MOD09A1) to control for that.[58] MOD13A1 has a spatial resolution of

121   500 m×500 m and a temporal resolution of 8 days. We used surface reflectance from

122   Band 3 and linearly interpolated values for days without measurements.

123   **2.5. Chemical Transport Model Outputs**

124   We used GEOS-Chem, a chemical transport model, to simulate ground-level $PM_{2.5}$

125   concentration. GEOS-Chem is a global 3-dimensional chemical transport model, which

126   uses meteorological inputs and emission inventories to simulate atmospheric components.

127   The details of GEOS-Chem is articulated somewhere else.[42] We performed a nested grid

128   simulation (Version 9.0.2) for North America at 0.500°×0.667° from 2005 to 2012, with

129   boundary conditions exported from a 2.0°×2.5° global simulation. Since meteorological

130   inputs at 0.500°×0.667° are not available from 2000 to 2004, we used 2.0°×2.5° outputs

131   instead. Based on previous studies and pilot testing, total $PM_{2.5}$ was defined as the sum of

132   nitrate, sulfate, elemental carbon, organic carbon, ammonium, sea salt aerosol, dust

133   aerosol and others (Table S2).[59]

134   In additional to providing ground-level $PM_{2.5}$ estimation, GEOS-Chem also simulates

135   vertical distribution of aerosol, which could be used for calibrating AOD. Previous

136   studies used GEOS-Chem to compute the percentage of ground-level aerosol in the total

137   column aerosol. This percentage was used in AOD calibration as a scaling factor.[29, 60]

7

138   Both studies utilized GEOS-Chem to provide both direct estimation for ground-level

139   $PM_{2.5}$ and a scaling factor to calibrate AOD.

140   **2.6. Meteorological Data**

141   Meteorological fields were obtained from NCEP North American Regional

142   Reanalysis data, which assimilates various data sources like land-surface, ship,

143   radiosonde, pibal, aircraft, satellite and others.[61] Meteorological data are daily estimate at

144   0.3° grid cells (about 32 km). In total 16 meteorological variables were used in this study.

145   They include air temperature, accumulated total precipitation, downward shortwave

146   radiation flux, accumulated total evaporation, planetary boundary layer height, low cloud

147   area fraction, precipitable water for the entire atmosphere, pressure, specific humidity at

148   2m, visibility, wind speed, medium cloud area fraction, high cloud area fraction, and

149   albedo. Wind speed was computed as the vector sum of u-wind (east-west component of

150   the wind) at 10m and v-wind (north-south component) at 10m.

151   **2.7. Aerosol Index Data**

152   Absorbing aerosol index (AAI) indicates the presence of absorbing aerosols in the

153   atmosphere. Major sources of absorbing aerosol include biomass burning and desert dust;

154   other minor sources could be volcanic ash.[62] AAI is informative for estimating absorbing

155   aerosols, such as organic carbon and soil dust.[63, 64] We used AAI Level 3 data products

156   from the Ozone Monitoring Instrument (OMI), where two algorithms are used in

157   retrieval. One is a near-UV algorithm, which retrieves UV aerosol index (OMI data

158   product OMAERUVd);[62, 64] and the other one uses multi-wavelength aerosol algorithm,

159   whose outputs include aerosol indexes at visible and UV range (OMI data product

8

160   OMAEROe).[65] Both algorithms have pros and cons, which have been discussed

161   previously.[66] Both data products are complementary and thus we used both. OMI AAI

162   data is available after October 2004. OMAERUVd data product has a spatial resolution of

163   1°; OMAEROe data product has a spatial resolution of 0.25°.

164   **2.8. Land-use terms**

165   Land-use terms serve as proxies for emissions and are used to capture variations at a

166   small spatial scale, which may not modeled by GEOS-Chem. The detailed process of

167   obtaining land-terms like elevation, road density, NEI (National Emissions Inventory)

168   emission inventory, population density, percentage of urban, and NDVI has been reported

169   somewhere else.[67] For vegetation coverage, we used percentage of vegetation from

170   NCEP North American Regional Reanalysis data and MODIS MOD13A2, a NDVI data

171   product.[68] MOD13A2 has a spatial resolution of 1 km×1 km and a temporal resolution of

172   16 days. We linearly interpolated NDVI values for days without measurements.

173   **2.9. Regional and Monthly Dummy**

174   Previous studies found the relationship between AOD and $PM_{2.5}$ have regional and

175   daily variation due to difference in meteorology and aerosol composition.[38, 69]

176   Atmospheric mechanism is complex and relationships between other variables could also

177   differ temporally and spatially. To account for that, we put monthly and regional dummy

178   variables. Regional dummy variable comes from major climate types in the United States

179   (Figure S3).[70] Since AOD-$PM_{2.5}$ relationship can change from day to day, daily dummy

180   variables would be ideal. However, training a neural network with 365 indicator variables

9

181   in addition to the other variables would be computationally intensive, and we used

182   monthly dummy variables as a compromise.

183   **3. Methods**

184   We trained a neural network with the above variables to monitored $PM_{2.5}$ from the

185   AQS network. The relationships between input variables and $PM_{2.5}$ could be highly

186   nonlinear with complex interactions. Neural networks have the potential to model any

187   type of nonlinearity.[71, 72] The details of the neural network, such as its structure and

188   training method were articulated in the supplementary material. All input variables

189   covered the entire study area, but some of them were not available in early years or had

190   higher proportions of missing values. Missing values were especially common in Terra

191   and Aqua AOD data. To deal with the missingness problem and different temporal

192   coverages, we adopted the following steps. We used a calibration method to fill in the

193   missing values in Aqua AOD data from 2003 to 2012 and Terra AOD data from 2001 to

194   2012 based on the association of GEOS-Chem outputs and land-use terms with non-

195   missing AOD.[56] For the other variables with a low fraction of missing values, we

196   interpolated at grid cells with missing values. Regarding temporal coverage, GEOS-

197   Chem outputs, land-use terms, MODIS outputs, and meteorological variables were

198   available throughout the study period. OMI data, Aqua AOD, and Terra AOD were

199   unavailable in earlier years. For years with one or more unavailable variables, we fitted

200   the model with the remaining available variables.

201   Most previous studies used only *in situ* variables for modeling. However, information

202   from neighboring cell can be informative as well. For example, nearby road density,

10

203   forest coverage and other land-use variables as well as nearby $PM_{2.5}$ measurements either

204   influence or correlate with local $PM_{2.5}$ measurements. They are informative for modeling

205   and can improve model performance. We accounted for spatial correlation by using

206   convolutional layers in the neural network.[73] A convolutional layer is computed by

207   applying a convolution kernel on an input layer. Values from neighboring cells are

208   combined through the use of the kernel function. The kernel takes the form a function

209   (e.g. weighted average with Gaussian weights based on distance) that produces a scalar

210   estimate from the multidimensional inputs. A convolution layer aggregates nearby

211   information and can simulate some form of autocorrelation. We included convolutional

212   layers for land-use terms and nearby $PM_{2.5}$ measurements as additional predictor

213   variables to account for spatial autocorrelation. Multiple convolution layers were

214   incorporated to allow the neural network to model even more complex autocorrelation or

215   possible interaction with other variables (Supplementary material). In addition to nearby

216   grid cells, observations from nearby days for the same grid cell can be also informative.

217   To incorporate this, we first fitted a neural network and obtained an initial prediction for

218     $PM_{2.5}$. We then computed temporal convolution layers and fitted the neural network

219   again with them (Figure S5).

220   To validate model results and avoid overfitting, we used ten-fold cross-validation, in

221   which all monitoring sites were randomly divided into 10%-90% splits. The model was

222   trained with 90% of data and predicted $PM_{2.5}$ at the remaining 10%. The same process

223   was repeated for other splits. Assembling predicted $PM_{2.5}$ at ten 10% testing sets yielded

224   predicted $PM_{2.5}$ for all the monitors. We computed correlation between predicted $PM_{2.5}$

11

225   and monitored $PM_{2.5}$. Spatial and temporal R^2s were also calculated. Details of

226   calculating R^2 have been specified in the supplementary material.

227   The trained neural network was then used to make daily $PM_{2.5}$ predictions for each

228   grid cell (1 km×1 km) for each day.

229   All programming was implemented in Matlab (version 2014a, The MathWorks, Inc.).

230   **4. Results**

231   To determine input variables, we compared models with different combinations of

232   input variables based on cross-validated total R^2. Model comparison indicated that (1) a

233   hybrid model performed better than any subset models (Figure S6); (2) scaling factor was

234   better to be incorporated as a separate input layer (Figure S7); (3) convolutional layers for

235   land-use variables and predicted $PM_{2.5}$ both improved model performance (Figures S6,

236   S8). Hence, input variables for the final model were GEOS-Chem outputs, Aqua and

237   Terra AOD, scaling factor, OMI AAIs, meteorological variables, NDVI, surface

238   reflectance, land-use terms, convolutional layers and regional/monthly dummy variables.

239   Table 1 presents model performance after conducting ten-fold cross-validation. Total R^2

240   between fitted and monitored $PM_{2.5}$ ranged from 0.74 to 0.88 and spatial R^2 was from

241   0.78 to 0.88. By season, the model usually performed better in summer, followed by

242   autumn, spring, and winter (Table S3). By region, regions in the Eastern United States

243   had the best model performance, followed by the Central United States. The Pacific and

244   Mountain regions had less satisfying model performance. We also found R^2 remained

245   high before 2008 and dropped after 2010 for sub-regions and the whole study area (Table

246   S4). We will discuss possible reasons later. Region name and division are from U.S.

12

247   census division (Table S1, Figure S2). In terms of spatial pattern, we found an east-west

248   gradient with model performing better in the Eastern and Central United States but less

249   satisfying in the western coast and the Mountain Region (Figure 1). Besides, some areas

250   in the Mountain Region (e.g. Great Basin and Colorado Plateau) with large variability in

251   elevation and surface type have relative low R^2 all the year round. Even in the Eastern

252   United States, where model performance is high in general, areas along Appalachian

253   Mountains and around Ozark Plateau have less satisfying model performance.

254   Figure 2 shows the spatial distribution of total $PM_{2.5}$ in the study area. The Eastern

255   United States generally had higher $PM_{2.5}$ levels than the Western part. Area around

256   Illinois and Ohio, areas around New York City and Philadelphia, and parts of the

257   Southeastern United States witnessed the heaviest $PM_{2.5}$ pollutions in the study area,

258   especially in summer. The San Joaquin Valley, Salt Lake City and Denver stood out in

259   the Western United States for their high $PM_{2.5}$ levels. Regarding temporal trend, the

260   national average dropped from 9.2 $\mu g/m^3$ in 2003 to 7.5 $\mu g/m^3$ 2012 (Figure 3). By

261   regions, the declining trend was predominantly in the Eastern United States, with largest

262   reduction occurring in East South Central Region (5.8 $\mu g/m^3$).

263   One additional way to validate our exposure estimates is to see if they can reproduce

264   the spatial autocorrelation in $PM_{2.5}$ concentrations. To do this, we calculated the

265   correlation among all pairs of $PM_{2.5}$ monitors in the EPA network, and plotted them as a

266   function of distance. We compared that to the same plot, but using our predicted $PM_{2.5}$

267   concentrations instead (Figure 4). The results show essential identical trends and

268   substantial overlap between the correlations of actual vs modeled $PM_{2.5}$ with distance.

269   **5. Discussion**

270   Our hybrid model incorporated existing $PM_{2.5}$ models as well as multiple variables

271   and achieved high out-of-sample R^2, averaging 0.84 (0.74~0.88 by year) over the study

272   period. The model performed better in some eastern regions, with an average out of

273   sample R^2 of 0.86~0.89 by region. To our best knowledge, our model performance

274   surpasses existing similar studies. Meanwhile, we predicted $PM_{2.5}$ daily concentrations at

275   nationwide 1 km×1 km grid cells from 2000 to 2012. As discussed below, this level of

276   resolution and coverage is an improvement over current $PM_{2.5}$ models and could be

277   beneficial to epidemiological studies. Epidemiologists could identify long-term and short-

278   term exposure of $PM_{2.5}$ in the whole continental United States at individual level, which

279   helps study adverse health effect of $PM_{2.5}$ with higher accuracy.

280   There are several advantages and innovations in our approach. First of all, our model

281   covered the whole United States with a spatial resolution of 1 km×1 km and a temporal

282   resolution of 1 day and achieved high R^2. As far as we know, if taking coverage,

283   resolution and model performance into consideration, our model performs better than

284   existing models. As mentioned in the introduction part, most $PM_{2.5}$ modeling work that

285   used AOD data focused on the AOD-$PM_{2.5}$ relationship, instead of making predictions.

286   For studies with similar research goal as ours, some of them have done AOD calibration

287   at global scale, but their estimation was long-term average[29] or annual average, with

288   some degree of bias (slope=0.68) and modest R^2 (R^2=0.65).[47] A previous study calibrated

289   AOD to daily monitored $PM_{2.5}$ in the Northeastern United States using mixed model and

290   achieved R^2 around 0.725~0.904.[31] A similar study used the similar method for the

291   Southeastern United States and achieved R^2 around 0.63 to 0.85.[32] Compared with both

292   regional models, our hybrid nationwide model performs slightly better in the

293   Northeastern United States and much better in the Southeastern United States (Table S6).

294   One reason is that aerosol formation in the Southeastern United States is affected by

295   biogenic isoprene emission from trees;[74] while isoprene emission from trees in the

296   Northeastern United States is less of a concern. Secondary organic aerosol that results

297   from isoprene has different absorption than other $PM_{2.5}$ components,[75] which is not well

298   captured by AOD. AAI provides some information about absorption profile, which helps

299   our hybrid model perform much better in the Southeast and almost the same or a little

300   better in the Northeast.

301   Second, our hybrid model integrated most variables that are known to be informative

302   to $PM_{2.5}$ modeling and improved model performance. This study reminds the importance

303   of hybrid framework and also proposes a possible neural network-based approach to

304   implement that. Atmospheric mechanism is complex and a single variable can only

305   capture an incomplete picture. For example, AOD measures the light extinction due to

306   aerosol in the whole atmosphere column. Different aerosols vary in terms of aerosol

307   absorption, which can affect AOD. More complexly, even the same aerosol type could

308   have various absorptions under different meteorological conditions and emission

309   features.[39] This discovery suggests that when modeling $PM_{2.5}$ with AOD data, AAI

310   (proxy for aerosol type), meteorological fields and emission profiles are also necessary.

311   There could be many unknown mechanisms intertwining with other variables. Multiple

312   variables are not redundant but complementary, which can recover the original picture of

313   atmospheric process and improve model performance to the best.

15

314   Third, we used convolutional layer in neural network for $PM_{2.5}$ modeling, which is an

315   innovation of our study. Primarily used in computer science, convolutional kernel is

316   placed over nearby pixels to produce a convolutional layer. Similarly, we used

317   convolutional layers in exposure assessment to aggregate variable values from nearby

318   grid cells or monitoring sites. Previous studies incorporated nearby information by using

319   nearby monitoring measurements, nearby road density or others, which were all pre-

320   specified. Our hybrid model takes multiple convolutional layers, which stand for various

321   ways of aggregating nearby information, and lets learning algorithm decide their relative

322   importance in the model. This approach is versatile and is able to model different

323   neighboring influences, as well as potential interactions with other variables.

324   Last but not least, we used AOD data with missing values been filled by some

325   calibration model. No further processing is required to deal with missing AOD data,

326   which could have been lengthy and cumbersome in previous studies.

327   For the east-west gradient in model performance (Figure 1), previous studies also

328   reported that correlation between MODIS AOD and ground-measured $PM_{2.5}$ is better in

329   the eastern part but poor in the western part, and they attributed poor model performance

330   to relative low $PM_{2.5}$ level and variability of terrain.[31, 41] This study lends support to both

331   statements. We quantified the relationship between model performance and elevation at

332   each monitoring site and found a negative correlation despite of much noise (Figure S10).

333   Similarly, a positive association exists between $PM_{2.5}$ level and model performance

334   (Figure S10), which implies that the drop of model performance after 2010 is probably

335   caused by substantive reduction in $PM_{2.5}$ level after 2010. This is also the reason why the

16

336   Mountain region, with low $PM_{2.5}$ level, has poor model performance. Lower level of

337    $PM_{2.5}$ means lower signal-to-noise ratio and model performance drops as model

338   uncertainty keeps constant. Besides, the reduction of sulfate is mainly responsible for

339   decreasing $PM_{2.5}$ level. Sulfate is better modeled in GEOS-Chem than other major

340   components like nitrate and ammonium,[76] so dropping sulfate causes unsatisfying model

341   performance. For the same reason, we saw less satisfying model performance in

342   California despite of its high $PM_{2.5}$ level, for the reason that California has high amount

343   of nitrate originated from vehicle exhaust compared with the Eastern United States. This

344   argument suggests that it would be informative to include sulfate in $PM_{2.5}$ modeling work

345   in the future.

346   Our model performance is still good even at low $PM_{2.5}$ levels. To prove that, we fitted

347   a spline regression of prediction $PM_{2.5}$ to measured $PM_{2.5}$. Linearity between measured

348   and predicted $PM_{2.5}$ holds when $PM_{2.5}$ level is below 70 $\mu g/m^3$ and become less obvious

349   above 80 $\mu g/m^3$ due to insufficient measurements (Figure 5). Bias at high concentration

350   is less of our concern, since there are few days with $PM_{2.5}$ level above 80 $\mu g/m^3$ in the

351   study area. If constraining to monitored $PM_{2.5}$ below 35 $\mu g/m^3$, the EPA daily standard

352   for $PM_{2.5}$, our hybrid model performed even better. Mean R^2 increased to 0.85; slope is

353   close 1; and intercept is close to 0 (Table S5). Good model performance at low $PM_{2.5}$

354   concentrations enables epidemiologists to estimate the adverse effect of $PM_{2.5}$ even

355   below EPA daily standard.

356   Figure 2 visualizes the spatial distribution of annual and seasonal average of $PM_{2.5}$.

357   There is also an east-west gradient of $PM_{2.5}$ level. The Eastern and Central United States

17

358 suffered relatively heavy PM$_{2.5}$ pollutions, except Appalachian Mountains, Florida

359 Peninsula, and some remote areas in the Northeast. The Southeastern United States,

360 especially Alabama and Georgia, witnessed high PM$_{2.5}$ level in summer and less

361 noticeably in spring and autumn, which results from isoprene emission from trees.

362 Isoprene emission from trees increases with temperature[74, 77] and peaks in hot summer.[78]

363 The Western United States had relatively low PM$_{2.5}$ levels, but the San Joaquin Valley,

364 Salt Lake City and Denver stood out for its abnormally high PM$_{2.5}$ level, which was also

365 featured by clear seasonality and high PM$_{2.5}$ level in winter. This is caused by

366 temperature inversion in winter which prevents atmospheric convection and trapped air

367 pollution near surface. For temporal trend, the Eastern and Central United States

368 witnessed a decreasing trend in PM$_{2.5}$ level (Figure 3), which is caused by reduction of

369 sulfur dioxide from power plant emission. For seasonal cycle, PM$_{2.5}$ level peaks in

370 summer in the Eastern and Central United States due to long-term transported sulfate

371 from power plants and isoprene-related organic carbon. The winter peaks are probably

372 caused by increased fuel burning for heat, and local temperature inversion that prevents

373 pollution dispersion.

374 Exposure assessments are essential for epidemiological studies. Traditional method of

375 exposure assessment relies on nearest monitors, which constraints the number of

376 available participants and introduces measurement errors. Besides, monitoring data from

377 some monitors are intermittent. Our PM$_{2.5}$ predictions have temporal resolution of 1 day

378 and spatial resolution of 1 km×1 km, which lifts the above limitations. Besides, our

379 hybrid model performs still well at low concentrations. Linearity between predicted and

380 monitored PM$_{2.5}$ still holds at low concentrations, without any signal of bias (Figure 5).

18

381   Cross-validated R^2 indicates good fit when daily $PM_{2.5}$ level is below 35 $\mu g/m^3$ (Table

382   S5), which enable epidemiologists to assess the adverse effect of $PM_{2.5}$ even below EPA

383   standard. In the long term, there is little discrepancy between long-term averages of

384   predicted and monitored $PM_{2.5}$, with difference below 1 $\mu g/m^3$ (Figure S9).

385   Some limitations remain. Our model requires quite a lot of variables, which limits the

386   application in other countries. This data-intensive approach could be difficulty in other

387   regions where public data is sparse. For regions with less data available, we might have

388   to make tradeoff between model performance and resolution. For example, instead of

389   daily prediction $PM_{2.5}$ at 1 km×1 km, we may model annual average of $PM_{2.5}$ or at coarse

390   spatial resolution. Besides, chemical profile of $PM_{2.5}$ is not available in this framework.

391   Previous epidemiological studies suggest various toxicities of $PM_{2.5}$ chemical

392   components,[79, 80] which is worthy of further investigation.

393

394

19

395   **Table 1. Cross-validated R^2 for the whole study area**

| Year	Total R^2	RMSE	Spatial R^2	RMSE	Temporal R^2	RMSE	Bias	Slope
2000	0.86	3.35	0.85	1.52	0.85	3.07	0.22	1.01
2001	0.84	3.58	0.86	1.40	0.83	3.35	0.22	1.01
2002	0.88	2.99	0.88	1.24	0.88	2.75	0.25	1.00
2003	0.88	2.80	0.87	1.21	0.88	2.57	0.23	1.00
2004	0.88	2.69	0.79	1.50	0.88	2.45	0.22	1.00
2005	0.88	2.94	0.84	1.45	0.89	2.66	0.27	1.00
2006	0.86	2.77	0.80	1.34	0.86	2.50	0.25	1.00
2007	0.87	2.95	0.83	1.31	0.87	2.72	0.21	1.00
2008	0.85	2.64	0.79	1.26	0.86	2.40	0.19	1.00
2009	0.82	2.73	0.81	1.09	0.82	2.54	0.21	1.00
2010	0.81	2.85	0.84	1.21	0.81	2.60	0.51	0.98
2011	0.81	2.83	0.81	1.11	0.81	2.60	0.38	0.99
2012	0.74	3.15	0.78	1.16	0.74	2.92	0.32	1.00
Mean	0.84	2.94	0.83	1.29	0.84	2.70	0.27	1.00

396
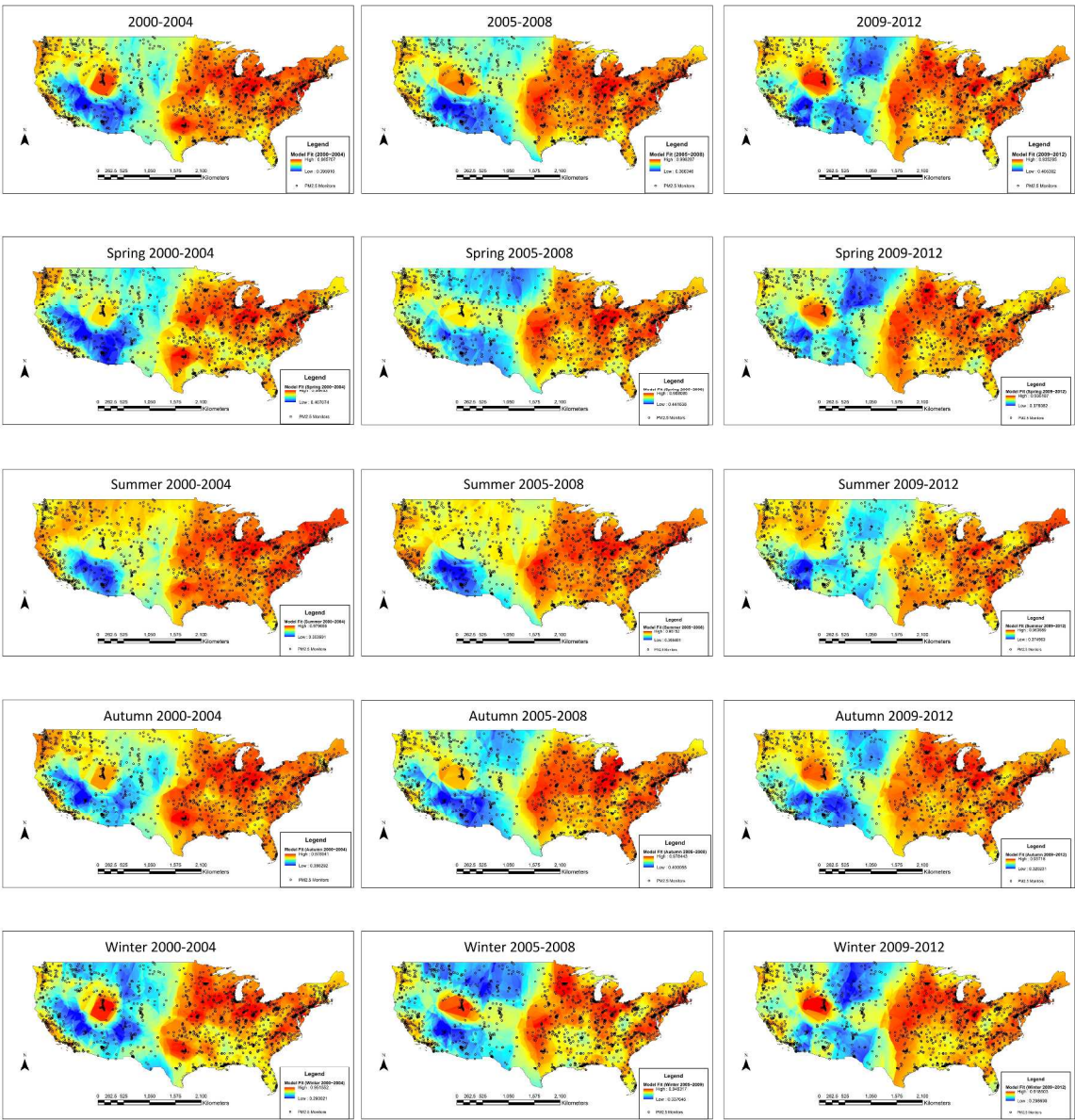
Figure 1. Model performance in the continental United States

We calculated total R^2 between monitored and predicted $PM_{2.5}$ for each monitoring site

and interpolated R^2 to places without monitors using Kriging interpolation. Spring was

defined as March to May; summer was defined as June to August; autumn was defined as

September to November; winter was from December to February of the next year (same

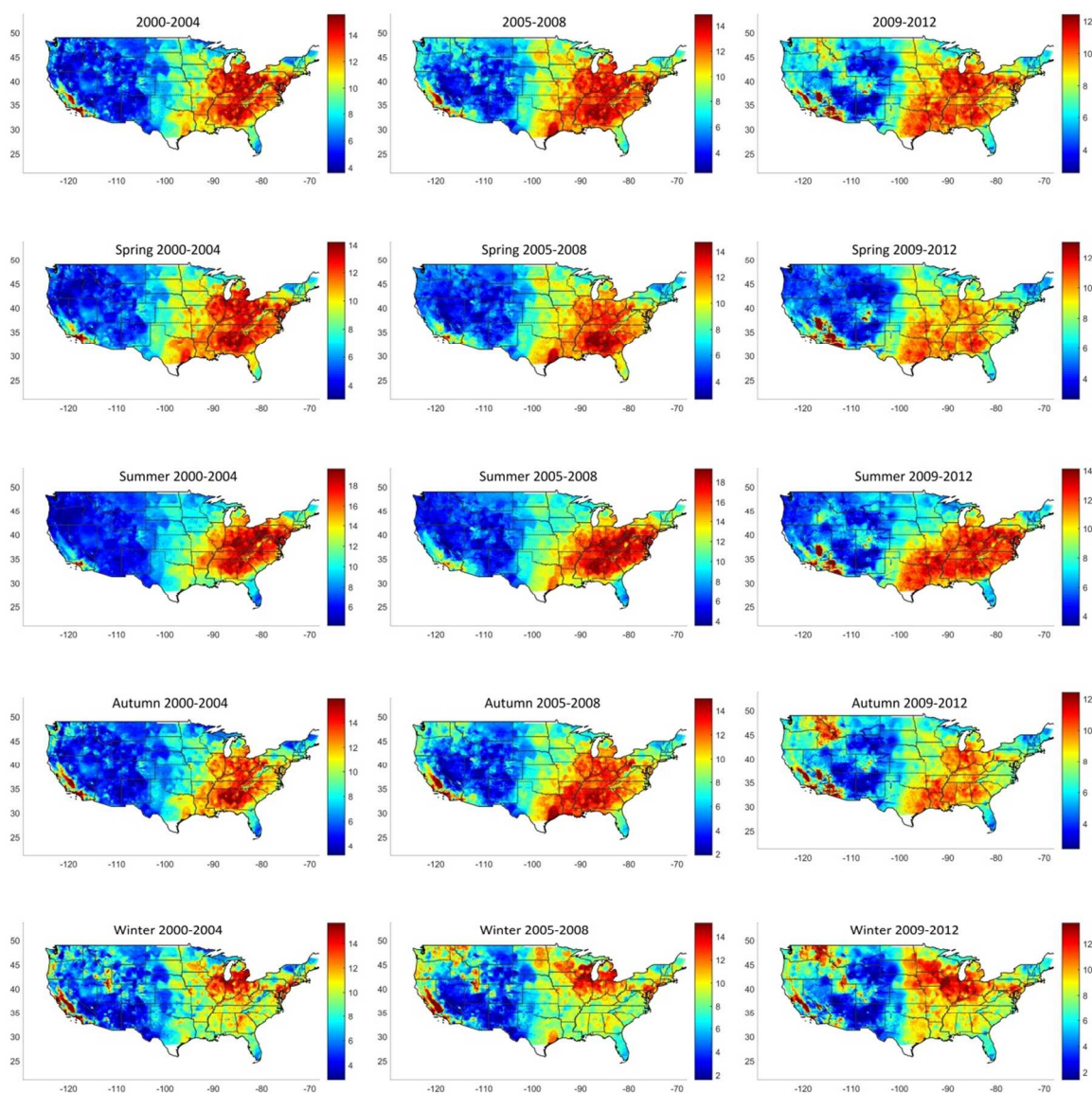below). Red color stands for high R^2 and blue color stands for low R^2.

21

404

Figure 2. Spatial distribution of predicted PM$_{2.5}$

The trained neural network predicted daily total PM$_{2.5}$ concentration at 1 km×1 km grid

cell in the study area. Red color stands for high concentrations and blue color stands for
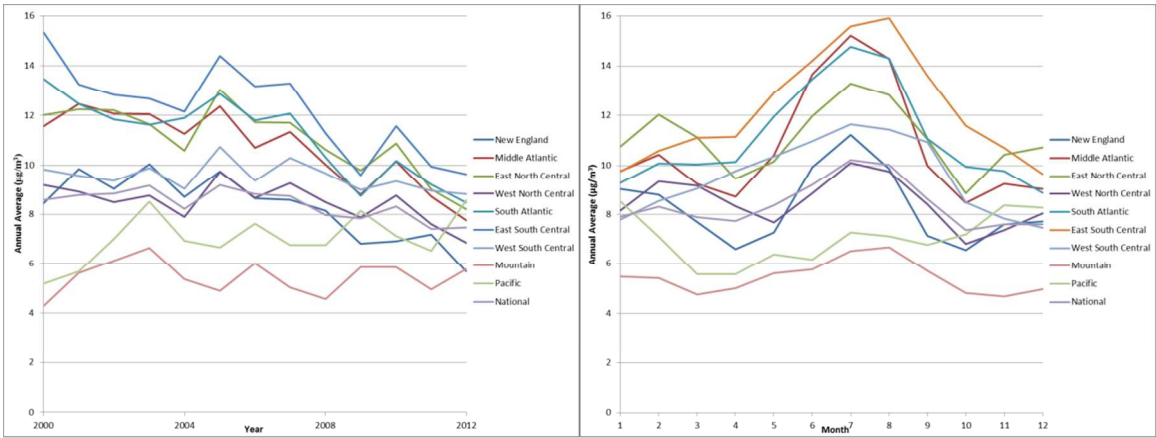
low concentrations.

409

22

410

Figure 3. Annual means by month of year and by region

Annual averages were computed by averaging all predicted $PM_{2.5}$ values at 1 km×1 km

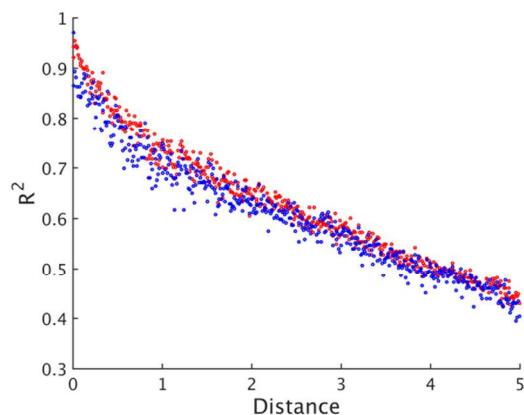grid cells in that region or in that month.

414

23

415

Figure 4. Relationship between correlation and distance between any two monitor sites

For 1,928 monitoring sites in the study area, we computed the correlation of $PM_{2.5}$ measurements and distance (in degree) between any two monitoring site pairs and plotted the between-site correlation versus between-site distance (red dots). We repeated the same process for predicted $PM_{2.5}$ and plotted the correlation of predicted $PM_{2.5}$ and monitored $PM_{2.5}$ between two site pairs versus distance (blue dots). This figure is for year 2012.

424

425

24

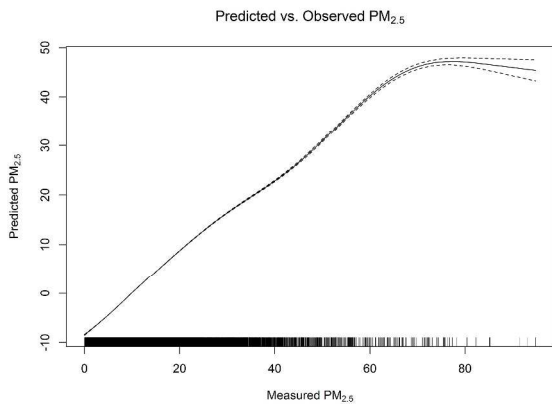Predicted vs. Observed PM$_{2.5}$

426

427   **Figure 5. Relationship between measured PM$_{2.5}$ and predicted PM$_{2.5}$**

428   We fit a penalized spline between measured PM$_{2.5}$ and predicted PM$_{2.5}$ without

429   specifying degree of freedom. This figure is for year 2009.

25

430   SUPPORTING INFORMATION

431   Maps of the study area, details on US census division, details on GEOS-Chem, details

432   on neural network and convolutional layers, details on calculating R^2, detailed results for

433   model comparison, cross-validated R^2 by region and by season, and model performance

434   at low concentrations.

435   AUTHOR INFOMRATION

436   **Corresponding Author**

437   *(Q.D.) Phone: 814-777-8202; email: qiandi@mail.harvard.edu

438   **Present Addresses**

439   [‡] Department of Geography and Environmental Development, Ben-Gurion University of

440   the Negev, Beer Sheva, P.O.B. 653, Israel

441   **Author Contributions**

442   The manuscript was written by Qian Di, edited and approved by all authors. All authors

443   have given approval to the final version of the manuscript.

26

450   REFERENCES

451   (1). Lim, S. S.; Vos, T.; Flaxman, A. D.; Danaei, G.; Shibuya, K.; Adair-Rohani, H.;

452   AlMazroa, M. A.; Amann, M.; Anderson, H. R.; Andrews, K. G. A comparative risk

453   assessment of burden of disease and injury attributable to 67 risk factors and risk factor

454   clusters in 21 regions, 1990–2010: a systematic analysis for the Global Burden of

455   Disease Study 2010. *The lancet* **2013,** *380*, (9859), 2224-2260.

456   (2). Slama, R.; Morgenstern, V.; Cyrys, J.; Zutavern, A.; Herbarth, O.; Wichmann, H.-

457   E.; Heinrich, J.; Group, L. S. Traffic-related atmospheric pollutants levels during

458   pregnancy and offspring's term birth weight: a study relying on a land-use regression

459   exposure model. *Environ. Health Persp.* **2007**, 1283-1292.

460   (3). Franklin, M.; Zeka, A.; Schwartz, J. Association between PM2. 5 and all-cause

461   and specific-cause mortality in 27 US communities. *J. Expo. Sci. Env. Epid.* **2007,** *17*,

462   (3), 279-287.

463   (4). Dominici, F.; Peng, R. D.; Bell, M. L.; Pham, L.; McDermott, A.; Zeger, S. L.;

464   Samet, J. M. Fine particulate air pollution and hospital admission for cardiovascular and

465   respiratory diseases. *Jama* **2006,** *295*, (10), 1127-1134.

466   (5). Gent, J. F.; Triche, E. W.; Holford, T. R.; Belanger, K.; Bracken, M. B.; Beckett,

467   W. S.; Leaderer, B. P. Association of low-level ozone and fine particles with respiratory

468   symptoms in children with asthma. *Jama* **2003,** *290*, (14), 1859-1867.

469   (6). Schwartz, J.; Dockery, D. W.; Neas, L. M. Is daily mortality associated

470   specifically with fine particles? *J. Air Waste Manage. (1995)* **1996,** *46*, 927-939.

471   (7). Halonen, J. I.; Lanki, T.; Yli-Tuomi, T.; Kulmala, M.; Tiittanen, P.; Pekkanen, J.

472   Urban air pollution and asthma and COPD hospital emergency room visits. *Thorax*

473   **2008**.

474   (8). Zanobetti, A.; Schwartz, J. The effect of fine and coarse particulate air pollution

475   on mortality: a national analysis. *Environ Health Perspect* **2009,** *117*, 898–903.

476   (9). Boldo, E.; Medina, S.; Le Tertre, A.; Hurley, F.; Mücke, H.-G.; Ballester, F.;

477   Aguilera, I. Apheis: Health impact assessment of long-term exposure to PM2. 5 in 23

478   European cities. *Eur. J. Epidemiol.* **2006,** *21*, (6), 449-458.

27

479   (10).   Schwartz, J. Harvesting and long term exposure effects in the relation
480   between air pollution and mortality. *Am. J. Epidemiol.* **2000,** *151*, 440-448.

481   (11).   Lippmann, M.; Ito, K.; Nadas, A.; Burnett, R. Association of particulate
482   matter components with daily mortality and morbidity in urban populations. *Res. Rep.*
483   *HEI* **2000**, (95), 5-72, discussion 73-82.

484   (12).   Sarnat, J. A.; Marmur, A.; Klein, M.; Kim, E.; Russell, A. G.; Sarnat, S.
485   E.; Mulholland, J. A.; Hopke, P. K.; Tolbert, P. E. Fine particle sources and
486   cardiorespiratory morbidity: an application of chemical mass balance and factor
487   analytical source-apportionment methods. *Environ. Health Persp.* **2008,** *116*, (4), 459.

488   (13).   Peng, R. D.; Bell, M. L.; Geyh, A. S.; McDermott, A.; Zeger, S. L.;
489   Samet, J. M.; Dominici, F. Emergency Admissions for Cardiovascular and Respiratory
490   Diseases and the Chemical Composition of Fine Particle Air Pollution. *Environ. Health*
491   *Persp.* **2009,** *117*, 957-963.

492   (14).   Peters, A.; Dockery, D. W.; Muller, J. E.; Mittleman, M. A. Increased
493   Particulate Air Pollution and the Triggering of Myocardial Infarction. *Circulation* **2001,**
494   *103*, 2810-2815.

495   (15).   Schwartz, J. Air pollution and hospital admissions for cardiovascular
496   disease in Tucson. *Epidemiology* **1997**, 371-377.

497   (16).   Schwartz, J.; Morris, R. Air pollution and hospital admissions for
498   cardiovascular disease in Detroit, Michigan. *Am. J. Epidemiol.* **1995,** *142*, (1), 23-35.

499   (17).   Pope, C. A.; Dockery, D. W. Health Effects of Fine Particulate Air
500   Pollution: Lines that Connect. *J. Air Waste Manage.* **2006,** *56*, 709-742.

501   (18).   Laden, F.; Schwartz, J.; Speizer, F. E.; Dockery, D. W. Reduction in fine
502   particulate air pollution and mortality: extended follow-up of the Harvard Six Cities
503   study. *Am. J. Resp. Crit. Care.* **2006,** *173*, 667–672.

504   (19).   Pinto, J. P.; Lefohn, A. S.; Shadwick, D. S. Spatial variability of PM2. 5 in
505   urban areas in the United States. *J. Air Waste Manage.* **2004,** *54*, (4), 440-449.

506   (20).   Beckerman, B. S.; Jerrett, M.; Martin, R. V.; van Donkelaar, A.; Ross, Z.;
507   Burnett, R. T. Application of the deletion/substitution/addition algorithm to selecting
508   land use regression models for interpolating air pollution measurements in California.
509   *Atmos. Environ.* **2013,** *77*, 172-177.

28

510 (21). Vienneau, D.; De Hoogh, K.; Beelen, R.; Fischer, P.; Hoek, G.; Briggs, D.

511 Comparison of land-use regression models between Great Britain and the Netherlands.

512 *Atmos. Environ.* **2010,** *44*, (5), 688-696.

513 (22). Aguilera, I.; Sunyer, J.; Fernández-Patier, R.; Hoek, G.; Aguirre-Alfaro,

514 A.; Meliefste, K.; Bomboi-Mingarro, M. T.; Nieuwenhuijsen, M. J.; Herce-Garraleta,

515 D.; Brunekreef, B. Estimation of Outdoor NO_x, NO_2, and BTEX Exposure in a Cohort

516 of Pregnant Women Using Land Use Regression Modeling. *Environ. Sci. Technol.* **2008,**

517 *42*, 815-821.

518 (23). Ghassoun, Y.; Ruths, M.; Löwner, M.-O.; Weber, S., Intra-urban variation

519 of ultrafine particles as evaluated by process related land use and pollutant driven

520 regression modelling. *Science of the Total Environment* **2015,** *536*, 150-160.

521 (24). Patton, A. P.; Zamore, W.; Naumova, E. N.; Levy, J. I.; Brugge, D.;

522 Durant, J. L., Transferability and generalizability of regression models of ultrafine

523 particles in urban neighborhoods in the Boston area. *Environmental science &*

524 *technology* **2015,** *49*, (10), 6051-6060.

525 (25). Hoek, G.; Beelen, R.; de Hoogh, K.; Vienneau, D.; Gulliver, J.; Fischer,

526 P.; Briggs, D., A review of land-use regression models to assess spatial variation of

527 outdoor air pollution. *Atmospheric Environment* **2008,** *42*, 7561-7578.

528 (26). Streets, D. G.; Canty, T.; Carmichael, G. R.; de Foy, B.; Dickerson, R. R.;

529 Duncan, B. N.; Edwards, D. P.; Haynes, J. A.; Henze, D. K.; Houyoux, M. R. Emissions

530 estimation from satellite retrievals: A review of current capability. *Atmos. Environ.*

531 **2013,** *77*, 1011-1042.

532 (27). Morain, S. A.; Budge, A. M. *Environmental Tracking for Public Health*

533 *Surveillance*. CRC Press: 2012.

534 (28). Chu, D. A.; Kaufman, Y.; Zibordi, G.; Chern, J.; Mao, J.; Li, C.; Holben,

535 B. Global monitoring of air pollution over land from the Earth Observing System-Terra

536 Moderate Resolution Imaging Spectroradiometer (MODIS). *J. Geophys. Res. Atoms.*

537 *(1984–2012)* **2003,** *108*, (D21).

538 (29). van Donkelaar, A.; Martin, R. V.; Brauer, M.; Kahn, R.; Levy, R.;

539 Verduzco, C.; Villeneuve, P. J. Global Estimates of Ambient Fine Particulate Matter

540   Concentrations from Satellite-Based Aerosol Optical Depth: Development and
541   Application. *Environ. Health Persp.* **2010,** *118*, 847-855.

542   (30).   Van Donkelaar, A.; Martin, R. V.; Park, R. J. Estimating ground-level
543   PM2. 5 using aerosol optical depth determined from satellite remote sensing. *J.*
544   *Geophys. Res. Atoms. (1984–2012)* **2006,** *111*, (D21).

545   (31).   Engel-Cox, J. A.; Holloman, C. H.; Coutant, B. W.; Hoff, R. M.
546   Qualitative and quantitative evaluation of MODIS satellite sensor data for regional and
547   urban scale air quality. *Atmos. Environ.* **2004,** *38*, (16), 2495-2509.

548   (32).   Wang, J.; Christopher, S. A. Intercomparison between satellite-derived
549   aerosol optical thickness and PM2. 5 mass: implications for air quality studies. *Geophys.*
550   *Res. Lett.* **2003,** *30*, (21).

551   (33).   Kloog, I.; Chudnovsky, A. A.; Just, A. C.; Nordio, F.; Koutrakis, P.;
552   Coull, B. A.; Lyapustin, A.; Wang, Y.; Schwartz, J. A new hybrid spatio-temporal
553   model for estimating daily multi-year $PM_{2.5}$ concentrations across northeastern USA
554   using high resolution aerosol optical depth data. *Atmos. Environ.* **2014,** *95*, 581-590.

555   (34).   Kloog, I.; Koutrakis, P.; Coull, B. A.; Lee, H. J.; Schwartz, J. Assessing
556   temporally and spatially resolved $PM_{2.5}$ exposures for epidemiological studies using
557   satellite aerosol optical depth measurements. *Atmos. Environ.* **2011,** *45*, 6267-6275.

558   (35).   Lee, M.; Kloog, I.; Chudnovsky, A.; Lyapustin, A.; Wang, Y.; Melly, S.;
559   Coull, B.; Koutrakis, P.; Schwartz, J. Spatiotemporal prediction of fine particulate
560   matter using high-resolution satellite images in the Southeastern US 2003–2011. *J.*
561   *Expo. Sci. Env. Epid.* **2015**.

562   (36).   Liu, Y.; Paciorek, C. J.; Koutrakis, P. Estimating Regional Spatial and
563   Temporal Variability of $PM_{2.5}$ Concentrations Using Satellite Data, Meteorology, and
564   Land Use Information. *Environ. Health Persp.* **2009,** *117*, 886-892.

565   (37).   Li, F.; Ramanathan, V. Winter to summer monsoon variation of aerosol
566   optical depth over the tropical Indian Ocean. *J. Geophys. Res. Atoms. (1984–2012)*
567   **2002,** *107*, (D16), AAC 2-1-AAC 2-13.

568   (38).   Schaap, M.; Apituley, A.; Timmermans, R.; Koelemeijer, R.; Leeuw, G. d.
569   Exploring the relation between aerosol optical depth and $PM_{2.5}$ at Cabauw, the
570   Netherlands. *Atmos. Chem. Phys.* **2009,** *9*, (3), 909-925.

571   (39).   Dubovik, O.; Holben, B.; Eck, T. F.; Smirnov, A.; Kaufman, Y. J.; King,

572   M. D.; Tanré, D.; Slutsker, I. Variability of absorption and optical properties of key

573   aerosol types observed in worldwide locations. *J. Atmos. Sci.* **2002,** *59,* (3), 590-608.

574   (40).   Hu, R.-M.; Sokhi, R.; Fisher, B. New algorithms and their application for

575   satellite remote sensing of surface PM2. 5 and aerosol absorption. *J. Aerosol Sci.* **2009,**

576   *40,* (5), 394-402.

577   (41).   Al-Saadi, J.; Szykman, J.; Pierce, R. B.; Kittaka, C.; Neil, D.; Chu, D. A.;

578   Remer, L.; Gumley, L.; Prins, E.; Weinstock, L. Improving national air quality forecasts

579   with satellite aerosol observations. *B. Am. Meteorol. Soc.* **2005,** *86,* (9), 1249-1261.

580   (42).   Bey, I.; Jacob, D. J.; Yantosca, R. M.; Logan, J. A.; Field, B. D.; Fiore, A.

581   M.; Li, Q.; Liu, H. Y.; Mickley, L. J.; Schultz, M. G. Global modeling of tropospheric

582   chemistry with assimilated meteorology: Model description and evaluation. *J. Geophys.*

583   *Res.* **2001,** *106,* 23073.

584   (43).   Byun, D. W.; Ching, J. *Science algorithms of the EPA Models-3*

585   *community multiscale air quality (CMAQ) modeling system*. United States

586   Environmental Protection Agency: Washington, DC, **1999**.

587   (44).   Bessagnet, B.; Hodzic, A.; Vautard, R.; Beekmann, M.; Cheinet, S.;

588   Honoré, C.; Liousse, C.; Rouil, L. Aerosol modeling with CHIMERE—preliminary

589   evaluation at the continental scale. *Atmos. Environ.* **2004,** *38,* 2803-2817.

590   (45).   Jun, M.; Stein, M. L. Statistical comparison of observed and CMAQ

591   modeled daily sulfate levels. *Atmos. Environ.* **2004,** *38,* 4427-4436.

592   (46).   Cordero, L.; Malakar, N.; Wu, Y.; Gross, B.; Moshary, F.; Ku, M.

593   Assessing satellite based $PM_{2.5}$ estimates against CMAQ model forecasts, *SPIE Remote*

594   *Sensing. Int. Soc. Opt. & Polym.*, **2013**, 8890 (Oct 17th),

595   (47).   van Donkelaar, A.; Martin, R. V.; Brauer, M.; Boys, B. L. Use of satellite

596   observations for long-term exposure assessment of global concentrations of fine

597   particulate matter. *Environ. Health Persp.* **2015,** *123,* (2), 135.

598   (48).   Di, Q.; Koutrakis, P.; Schwartz, J. A Hybrid Prediction Model for $PM_{2.5}$

599   Mass and Components Using a Chemical Transport Model and Land Use Regression.

600   *Atmos. Environ.* **2016**, 131, 390-399.

601   (49).   King, M. D.; Kaufman, Y. J.; Menzel, W. P.; Tanre, D. Remote sensing of

602   cloud, aerosol, and water vapor properties from the Moderate Resolution Imaging

603   Spectrometer (MODIS). *IEEE T. Geosci. Remote* **1992,** *30*, (1), 2-27.

604   (50).   Salomonson, V. V.; Barnes, W.; Maymon, P. W.; Montgomery, H. E.;

605   Ostrow, H. MODIS: Advanced facility instrument for studies of the Earth as a system.

606   *IEEE T. Geosci. Remote* **1989,** *27*, (2), 145-153.

607   (51).   Remer, L. A.; Kaufman, Y. J.; Tanré, D.; Mattoo, S.; Chu, D. A.; Martins,

608   J. V.; Li, R.-R.; Ichoku, C.; Levy, R. C.; Kleidman, R. G.; et al. The MODIS Aerosol

609   Algorithm, Products, and Validation. *J. Atmos. Sci.* **2005,** *62*, 947-973.

610   (52).   Chudnovsky, A.; Lyapustin, A.; Wang, Y.; Schwartz, J.; Koutrakis, P.

611   Analyses of high resolution aerosol data from MODIS satellite: a MAIAC retrieval,

612   southern New England, US. *First International Conference on Remote Sensing and*

613   *Geoinformation of the Environment* **2013,** 8795 (Aug 5th).

614   (53).   Lyapustin, A.; Martonchik, J.; Wang, Y.; Laszlo, I.; Korkin, S. Multiangle

615   implementation of atmospheric correction (MAIAC): 1. Radiative transfer basis and

616   look-up tables. *J. Geophys. Res. Atoms. (1984–2012)* **2011,** *116*, (D3).

617   (54).   Lyapustin, A.; Wang, Y.; Laszlo, I.; Kahn, R.; Korkin, S.; Remer, L.;

618   Levy, R.; Reid, J. Multiangle implementation of atmospheric correction (MAIAC): 2.

619   Aerosol algorithm. *J. Geophys. Res. Atoms. (1984–2012)* **2011,** *116*, (D3).

620   (55).   van Donkelaar, A.; Martin, R. V.; Park, R. J. Estimating ground-level

621     $PM_{2.5}$ using aerosol optical depth determined from satellite remote sensing. *J. Geophys.*

622   *Res.* **2006,** *111*.

623   (56).   Di, Q.; Schwartz, J. Using Chemical Transport Model to Fill in the

624   Missingness of Satellite-Based AOD. *Atmos. Environ.* (In review).

625   (57).   Drury, E.; Jacob, D. J.; Wang, J.; Spurr, R. J.; Chance, K. Improved

626   algorithm for MODIS satellite retrievals of aerosol optical depths over western North

627   America. *J. Geophys. Res. Atoms. (1984–2012)* **2008,** *113*, (D16).

628   (58).   Vermote, E. MOD09A1 MODIS/Terra Surface Reflectance 8-Day L3

629   Global 500m SIN Grid V006. *NASA EOSDIS Land Processes DAAC*. **2015.**

630   (59).   Isakov, V.; Touma, J.; Touma, J.; Khlystov, A.; Sattler, M.; Devanathan,

631   S.; Devanathan, S.; Engel-Cox, J.; Weber, S.; McFarland, M.; et al. Estimating Fine

                                                         32

632   Particulate Matter Component Concentrations and Size Distributions Using Satellite-

633   Retrieved Fractional Aerosol Optical Depth: Part 2—A Case Study. *J. Air Waste*

634   *Manage.* **2007,** *57*, 1360-1369.

635   (60).   Liu, Y. Mapping annual mean ground-level $PM_{2.5}$ concentrations using

636   Multiangle Imaging Spectroradiometer aerosol optical thickness over the contiguous

637   United States. *J. Geophys. Res.* **2004,** *109*.

638   (61).   Kalnay, E.; Kanamitsu, M.; Kistler, R.; Collins, W.; Deaven, D.; Gandin,

639   L.; Iredell, M.; Saha, S.; White, G.; Woollen, J.; et al. The NCEP/NCAR 40-Year

640   Reanalysis Project. *B. Am. Meteorol. Soc.* **1996,** *77*, 437-471.

641   (62).   Herman, J.; Bhartia, P.; Torres, O.; Hsu, C.; Seftor, C.; Celarier, E. Global

642   distribution of UV-absorbing aerosols from Nimbus 7/TOMS data. *J. Geophys. Res*

643   **1997,** *102*, (16), 911-16.

644   (63).   Tegen, I.; Werner, M.; Harrison, S.; Kohfeld, K. Relative importance of

645   climate and land use in determining present and future global soil dust emission.

646   *Geophys. Res. Lett.* **2004,** *31*, (5).

647   (64).   Torres, O.; Bhartia, P.; Herman, J.; Ahmad, Z.; Gleason, J. Derivation of

648   aerosol properties from satellite measurements of backscattered ultraviolet radiation:

649   Theoretical basis. *J. Geophys. Res. Atoms. (1984–2012)* **1998,** *103*, (D14), 17099-

650   17110.

651   (65).   Stein-Zweers, D.; Veefkind, P. OMI/Aura Multi-wavelength Aerosol

652   Optical Depth and Single Scattering Albedo Daily L3 Global 0.25x0.25 deg Lat/Lon

653   Grid,version 003. *NASA Goddard Space Flight Center* **2012**.

654   (66).   Torres, O.; Tanskanen, A.; Veihelmann, B.; Ahn, C.; Braak, R.; Bhartia,

655   P. K.; Veefkind, P.; Levelt, P. Aerosols and surface UV products from Ozone

656   Monitoring Instrument observations: An overview. *J. Geophys. Res. Atoms. (1984–*

657   *2012)* **2007,** *112*, (D24).

658   (67).   Kloog, I.; Nordio, F.; Coull, B. A.; Schwartz, J. Incorporating Local Land

659   Use Regression And Satellite Aerosol Optical Depth In A Hybrid Model Of

660   Spatiotemporal $PM_{2.5}$ Exposures In The Mid-Atlantic States. *Environ. Sci. Technol.*

661   **2012,** *46*, 11913-11921.

662   (68).   Didan, K. MOD13A2 MODIS/Terra Vegetation Indices 16-Day L3 Global

663   1km SIN Grid V006. *NASA EOSDIS Land Processes DAAC* **2015**.

664   (69).   Lee, H.; Liu, Y.; Coull, B.; Schwartz, J.; Koutrakis, P. A novel calibration

665   approach of MODIS AOD data to predict PM2. 5 concentrations. *Atmos. Chem. Phys*

666   **2011,** *11*, (15), 7991-8002.

667   (70).   Kottek, M.; Grieser, J.; Beck, C.; Rudolf, B.; Rubel, F. World map of the

668   Köppen-Geiger climate classification updated. *Meteorol. Z.* **2006,** *15*, (3), 259-263.

669   (71).   Bishop, C. M. *Neural networks for pattern recognition*. Oxford university

670   press: **1995**.

671   (72).   Haykin, S.; Network, N. A comprehensive foundation. *Neural Networks*

672   **2004,** *2*, (2004).

673   (73).   LeCun, Y.; Bengio, Y. Convolutional networks for images, speech, and

674   time series. *The handbook of brain theory and neural networks* **1995,** *3361*, (10).

675   (74).   Sharkey, T. D.; Wiberley, A. E.; Donohue, A. R. Isoprene emission from

676   plants: why and how. *Ann. Bot.* **2008,** *101*, (1), 5-18.

677   (75).   Claeys, M.; Graham, B.; Vas, G.; Wang, W.; Vermeylen, R.; Pashynska,

678   V.; Cafmeyer, J.; Guyon, P.; Andreae, M. O.; Artaxo, P. Formation of secondary

679   organic aerosols through photooxidation of isoprene. *Science* **2004,** *303*, (5661), 1173-

680   1176.

681   (76).   Park, R. J.; Jacob, D. J.; Field, B. D.; Yantosca, R. M.; Chin, M. Natural

682   and transboundary pollution influences on sulfate-nitrate-ammonium aerosols in the

683   United States: Implications for policy. *J. Geophys. Res. Atoms. (1984–2012)* **2004,** *109*,

684   (D15).

685   (77).   Sharkey, T. D.; Singsaas, E. L.; Vanderveer, P. J.; Geron, C. Field

686   measurements of isoprene emission from trees in response to temperature and light. *Tree*

687   *Physiol.***1996,** *16*, (7), 649-654.

688   (78).   Geron, C.; Harley, P.; Guenther, A. Isoprene emission capacity for US tree

689   species. *Atmos. Environ.***2001,** *35*, (19), 3341-3352.

690   (79).   Franklin, M.; Koutrakis, P.; Schwartz, P. The role of particle composition

691   on the association between $PM_{2.5}$ and mortality. *Epidemiology* **2008,** *19*, (5), 680-9.

692   (80).   Dai, L.; Zanobetti, A.; Koutrakis, P.; Schwartz, J. D. Associations of fine

693   particulate matter species with mortality in the United States: a multicity time-series

694   analysis. *Environ. Health Persp.***2014,** *122*, 837.

35